

Inner southern magnetosphere observation of Mercury via SERENA ion sensors in BepiColombo mission

Received: 24 March 2022

Accepted: 14 November 2022

Published online: 30 November 2022



A list of authors and their affiliations appears at the end of the paper

Mercury's southern inner magnetosphere is an unexplored region as it was not observed by earlier space missions. In October 2021, BepiColombo mission has passed through this region during its first Mercury flyby. Here, we describe the observations of SERENA ion sensors nearby and inside Mercury's magnetosphere. An intermittent high-energy signal, possibly due to an interplanetary magnetic flux rope, has been observed downstream Mercury, together with low energy solar wind. Low energy ions, possibly due to satellite outgassing, were detected outside the magnetosphere. The dayside magnetopause and bow-shock crossing were much closer to the planet than expected, signature of a highly eroded magnetosphere. Different ion populations have been observed inside the magnetosphere, like low latitude boundary layer at magnetopause inbound and partial ring current at dawn close to the planet. These observations are important for understanding the weak magnetosphere behavior so close to the Sun, revealing details never reached before.

Planet Mercury was visited in the past by only two satellites: Mariner-10 (3 flybys in 1974 / 1975)¹, and 'MErcury Surface, Space ENvironment, GEochemistry, and Ranging' (MESSENGER), which orbited the planet from 2011 to 2015². Concerning environment, Mariner-10 discovered the existence of a weak internal dipolar magnetic field;³ MESSENGER allowed to quantify the magnetic dipole moment (190 nT R_M^3), offset northward by about 0.2 R_M ,⁴ and to depict a dynamic magnetosphere, strongly coupled with the solar wind conditions, and a high reconnection rate⁵. Anyway, none of the previous missions was able to fully explain the planet and environment peculiarities, so that many questions are still unsolved. The ESA-JAXA BepiColombo (BC) mission was launched in October 2018, having onboard a large set of instruments to better study the characteristics of this planet, so close to the Sun⁶. BC is composed by two elements: MPO (Mercury Planetary Orbiter, ESA), and Mio (Mercury Magnetospheric Orbiter, JAXA). After traveling in the interplanetary space for the first three years, BC passed by its target planet Mercury for the first time on 1st October 2021. The final orbital insertion of the two elements MPO and Mio will take place at the end of 2025: MPO will be inserted in a polar orbital path, at beginning between 480 and 1500 km; Mio will have a polar orbital path as well, at beginning between 590 and 11640 km. Before the beginning of the

nominal phase, it will perform six Mercury Flybys in total⁷. In the actual cruise configuration of the composite spacecraft, not all BC instruments can operate. In particular, the 'Search for Exospheric Refilling and Emitted Natural Abundances' (SERENA) suite of four units, devoted to the study of the ion and neutral particle populations around the planet⁸, has the possibility to perform scientific measurements during cruise via two units, 'Planetary Ion CAMera' (PICAM) and 'Miniaturized Ion Precipitation Analyzer' (MIPA), both devoted to the observation of positive ions coming from the solar wind as well as from the planet's environment. PICAM and MIPA have a 3D Field-of-View (FoV) $< 2\pi$, with the boresight pointing perpendicular to the Sun direction (see Supplementary Information for details). Both sensors are nominally able to detect the solar wind in their extreme lateral views: in this case, due to the sensitivity trend versus angle from the boresight, only PICAM is able to clearly detect the solar wind signal. Moreover, the two sensors together observe plasma regimes over a wide energy range, covering both solar wind and planetary ion populations, outside and inside Mercury's magnetosphere. Short technical feature descriptions of PICAM (Supplementary Fig. 1, Supplementary Table 1), and MIPA (Supplementary Fig. 2, Supplementary Table 2) are given in the Supplementary Information.

✉ e-mail: stefano.orsini@inaf.it

In the following, the timing of the observations along the BC trajectory near-by Mercury is described, and the PICAM and MIPA data are shown.

Here we show that the trajectory of the first Mercury flyby (MFB1) covers regions in the southern hemisphere at low altitudes not explored by previous missions. The collected data allow showing ion energy distributions at the bow shock and closer to Mercury in the southern hemisphere. Such preliminary raw data reveal very interesting solar wind features and magnetospheric plasma regimes, giving a clear evidence of the potentiality of BC instrumentation. MFB1 is a first relevant step versus a comprehensive understanding of the environment around Mercury.

Results

1. BepiColombo trajectory and region traversals.

The BC MFB1 occurred between the 1st and the 2nd of October 2021. The Mercury Solar Magnetospheric coordinated system (MSM) is centered on the planetary magnetic dipole with the X -axis positive in the solar direction and an offset northward along the MSM Z -axis by 480 km (about 0.2 R_M), parallel to the planetary rotation axis⁵. The Y -axis is positive opposite to the direction of Mercury's orbital velocity which completes the right-handed MSM system. The spacecraft approached the planet from the dusk flank, the magnetosheath and near magnetotail, and exited the magnetosphere in the dawn dayside, again crossing the magnetosheath (Fig. 1). The closest approach occurred on October 1st, at 23:34 UT at an altitude of 199 km and Z_{MSM} about $-0.7 R_M$ in the nightside. As shown in Fig. 2, PICAM operated during 4 distinct time periods and observed the solar wind ion flux (Panel a, insets 1 and 4), the inbound magnetosheath, and the inner magnetosphere (Panel a, inset 2), and the region upstream of the bow shock (Panel a, inset 3), while MIPA operated continuously from 22:35 UT to 23:56 UT, and observed the magnetosheath adjacent to the tail, the inner magnetosphere and the outbound magnetopause and bow shock (Panel b).

2. Solar wind observations.

The solar wind was not always visible to PICAM and MIPA during the cruise, depending on the FoV direction (the FoV edge being about 30° off the Sun direction). Nevertheless, while approaching Mercury, PICAM was able to see part of the solar wind distribution that appeared to be quite warm, dense, and at low energy (peaking at about 600 eV). Between 19:00 UT and 21:00 UT, at a distance of about $25 R_M$ from Mercury center, in the dusk side, the spacecraft rotated and the PICAM boresight moved from the $-Z_{MSM}$ direction, i.e., the southern hemisphere to $+Z_{MSM}$ in the northern hemisphere (see Fig. 3). In doing so, PICAM FoV passed through the $-Y_{MSM}$ direction (i.e., moving to the same direction as the planet moves pointing along the ecliptic plane toward the bow shock).

During this time-period, PICAM observed clear intermittent features (with a time scale of a few minutes) at high energies (above 1 keV, Fig. 4a). Actually, their appearance is clearly associated with PICAM's FoV pointing towards the bow shock, as opposed to the solar wind direction, but the possibility that these intermittent structures could be related to a source from the bow-shock⁹ is hardly applicable by considering that the vantage point is too far away from the bow shock itself. A combined analysis with magnetic field data from BC/MAG (MPO magnetometer) would be needed, to verify that these keV particles could be associated with the passage of an interplanetary magnetic flux rope with its axis oriented along the Y -axis. In this case, MAG should observe the typical signature of this structure, i.e., an increase of the average magnetic field magnitude (with respect to the main background field), a decrease of the variance of magnetic field fluctuations, and a smooth rotation of one of the field components. Such findings have a chance to be also validated by means of Solar Orbiter (SolO) magnetic field observations. In fact, SolO¹⁰ was located at a distance of 0.64 AU from the Sun (0.26 AU ahead BC) and the two spacecraft were reasonably radially aligned, longitudinally separated by less than 10° , and lying on the same side of the heliospheric current sheet. Details of the results of this analysis will be reported in a forthcoming paper, as soon as the MAG data will be confirmed and officially validated. The actual effect over

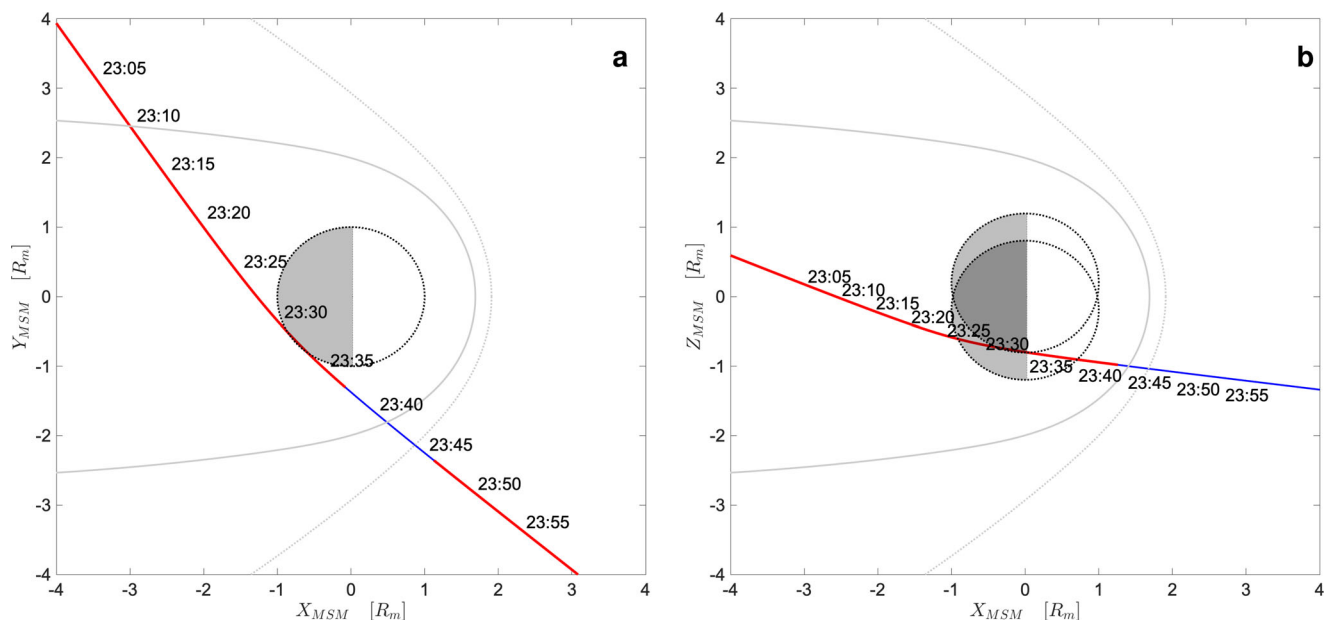


Fig. 1 | Trajectory of BepiColombo during MFB1. The trajectory of BepiColombo during the interval of interest, **a** in the X_{MSM} - Y_{MSM} plane, **b** in the X_{MSM} - Z_{MSM} plane. The solid gray line represents the magnetopause surface, while the dashed gray line

correspond to the bow shock surface. Red lines correspond to the operational time of PICAM and MIPA sensors. Time labels are shown progressively along the trajectory. BC position data are given in the Source Data file.

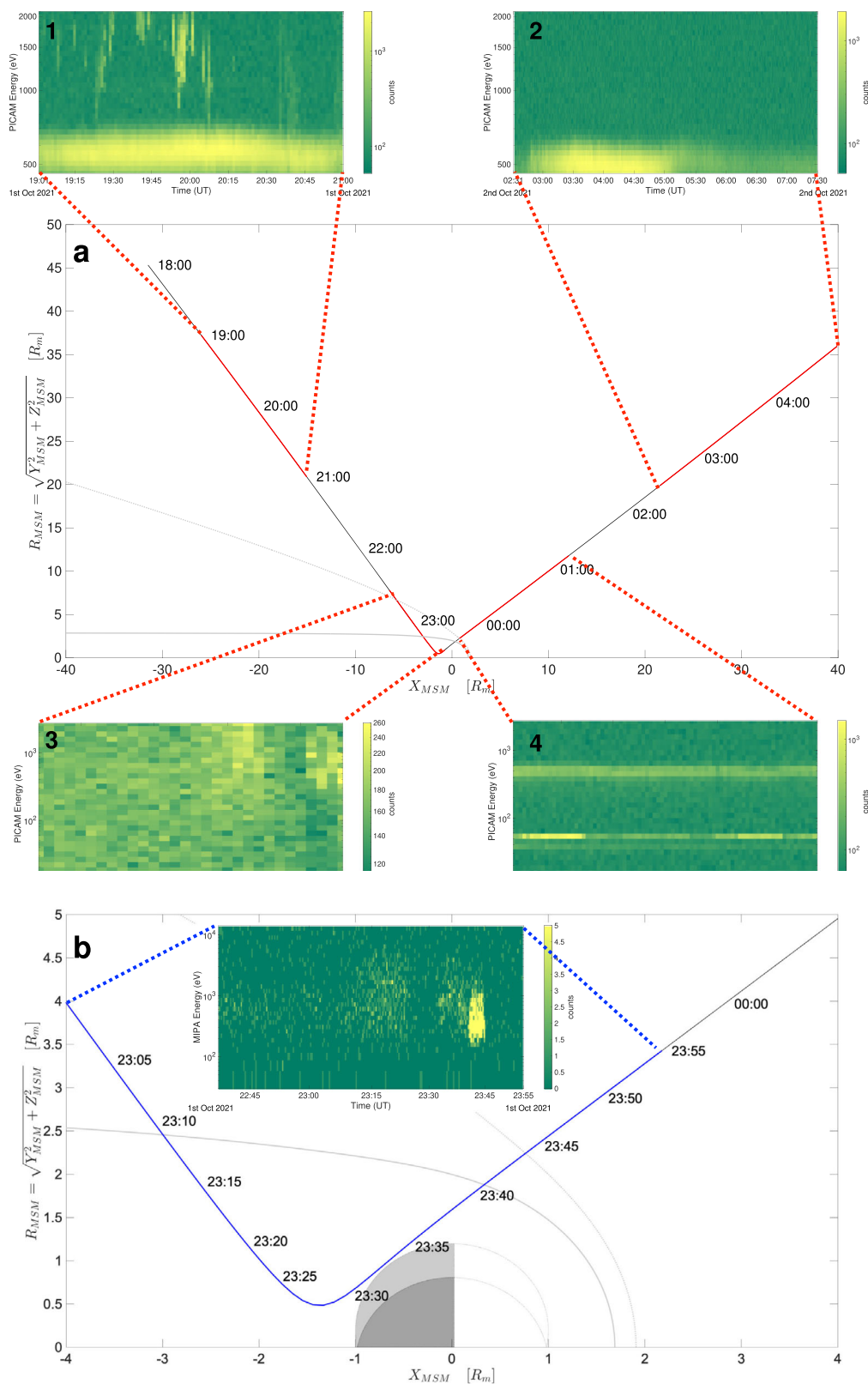


Fig. 2 | Trajectory of BepiColombo and SERENA observations during MFB1. The trajectory of BepiColombo during the interval of interest in the X_{MSM} - R_{MSM} plane. **a** PICAM observations, **b** MIPA observations. The solid gray line represents the magnetopause surface, while the dashed gray line corresponds to the bow shock surface^{25,26}. Red lines in **a** correspond to the operational time of PICAM, blue line in

b corresponds to MIPA operation time. Time labels are shown progressively along the trajectory. Insets 1–4 in **a** show PICAM spectrograms for each specific time window, while the inset in **b** displays MIPA spectrograms. Color bars report ion counts in each specific time interval. BC position data are given in the Source Datas file.

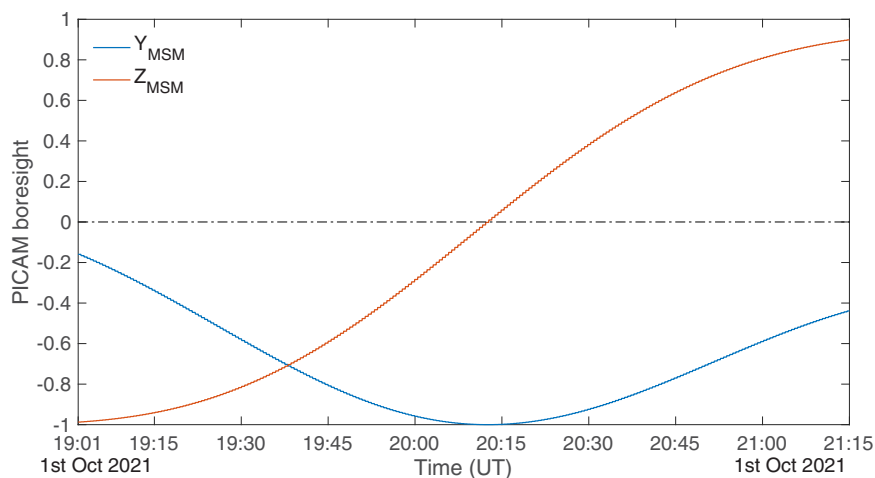


Fig. 3 | PICAM boresight components along Y_{MSM} and Z_{MSM} versus UT during MFB1. The Y_{MSM} and Z_{MSM} components of the PICAM boresight are plotted versus UT for the time interval from 19:00 UT to 21:15 UT of the 1st of October, 2021. The

blue line refers to the Y_{MSM} component, while the red line refers to the Z_{MSM} component. The horizontal dashed-dotted black line identifies the zero.

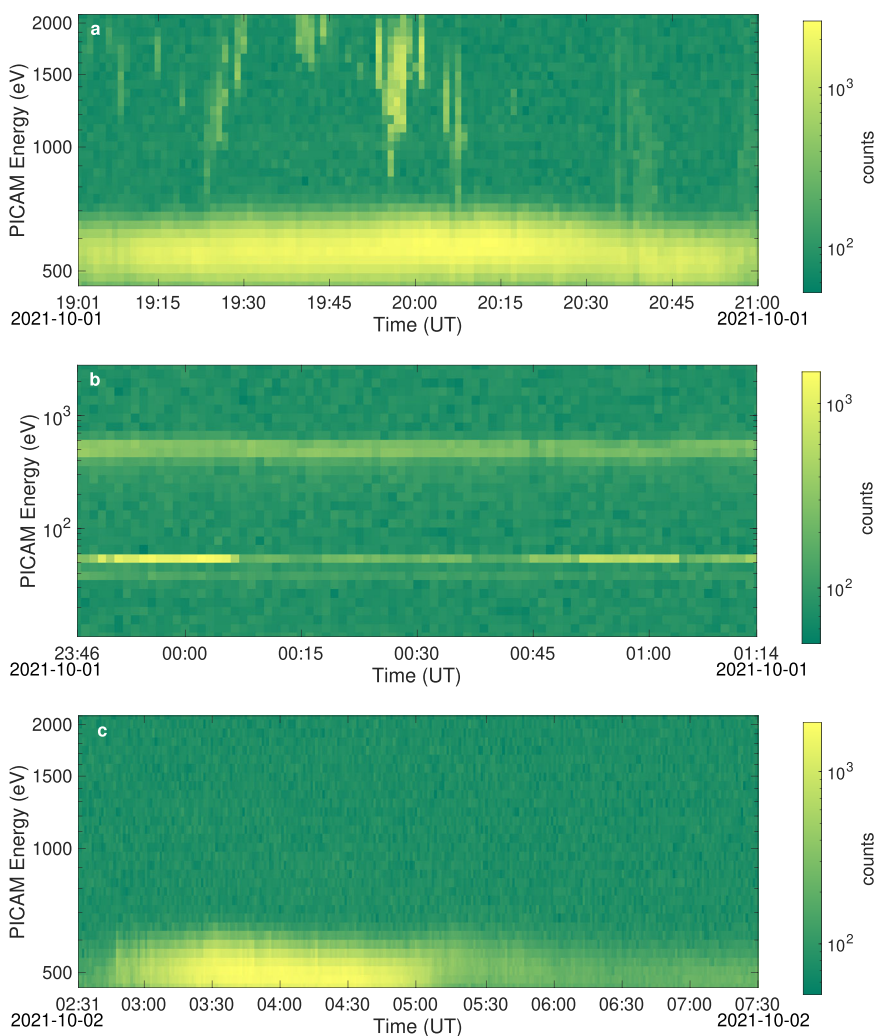


Fig. 4 | MFB1 PICAM spectrograms outside Mercury's magnetosphere. The spectrograms obtained by PICAM observations during the different time intervals: **a** from 19:01 UT to 21:00 UT on the 1st of October, 2021, **b** from 23:46 UT on the 1st

of October, 2021, to 01:14 UT on the 2nd of October, 2021, **c** from 02:31 UT to 07:30 UT on the 2nd of October, 2021. Color bars report ion counts in each specific time interval.

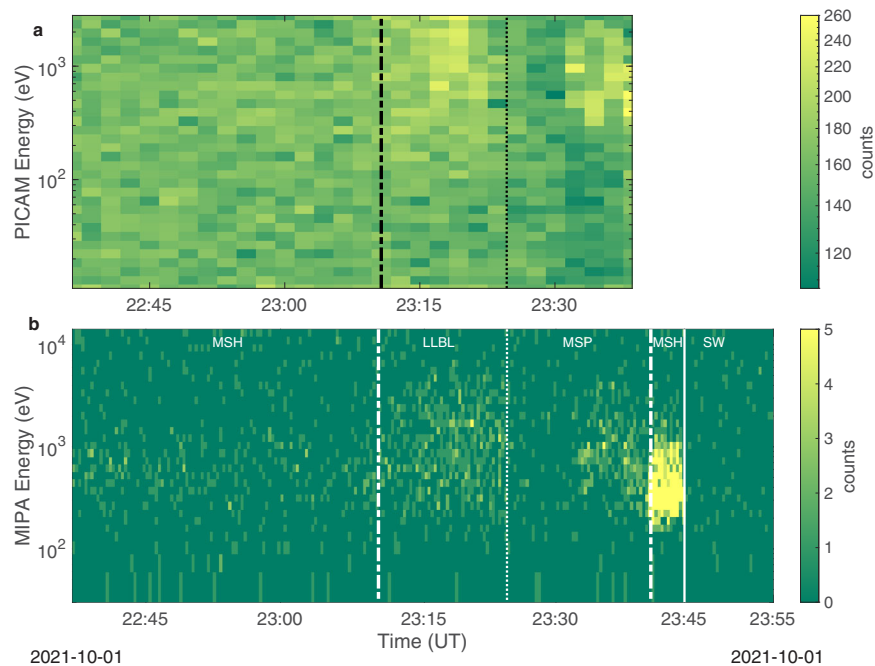


Fig. 5 | MFB1 PICAM and MIPA spectrograms inside Mercury's magnetosphere. The spectrograms obtained by **a** PICAM observations and **b** MIPA measurements in the inner magnetosphere of Mercury. The dashed-dotted lines refer to the expected inbound and outbound magnetopause crossings, the dotted lines refer to the observed transition from low latitude boundary layer to the magnetospheric dusk

lobe, while the solid line in **b** marks the bow shock crossing. Labels refer to the different regions crossed by the spacecraft, specifically: magnetosheath (MSH), low latitude boundary layer (LLBL), inner magnetosphere (MSP), and solar wind (SW). Color bars report ion counts in each specific time interval.

the Mercury environment would have been the subject of an interesting study, but unfortunately the solar wind structure vanished well before the flyby, and any possible internal effect was not observed. It likely produces enhanced flux transfer events and magnetic reconnection sites, together with small substorm-like activity in the nightside of the Hermean magnetosphere. However, as we will show in the next section the Mercury's magnetosphere was in quiet conditions, thus suggesting that it reconfigured after the passage of the flux rope. Such kind of events will be further investigated during the nominal mission (after satellite orbital insertions, in late 2025), when Mio will observe the solar wind conditions and simultaneously MPO will record any internal reaction. The solar wind observed upstream, on the dawn side of Mercury (Fig. 4c), shows a similar average energy, but appears to be more variable with a sharp drop in intensity after 5 UT, indicating an unstable condition. Just behind Mercury's bow shock, PICAM performed ion observations within an extended energy range, including lower energies. The solar wind energy was somewhat low, corresponding to about 550 eV (Fig. 4b). Two signals at even lower energies (the bands at 38 eV and 60 eV) were clearly observed, with a variable density on time scales of 30 min, with sunward and anti-sunward directions, respectively. Further investigation is needed by cumulating more events statistically significant with different environmental conditions and satellite orientations, in order to clarify whether this signal is originating from Mercury's interaction with the solar wind, or alternatively it is induced by spacecraft outgassing¹¹. The Mass Spectrum Analyzer (MSA), a unit of the MPPE (Mercury Plasma Particle Experiment) consortium onboard BC-Mio, confirms the existence of a distinct double-band feature at low energies and that O⁺ is the dominant ion species. The simultaneous observation by two separate BC instruments of such a low-energy signal excludes the possibility that it could come from instrumental effects. The persistent presence of outgassing material around spacecraft was

discovered several years ago in the surrounding of Rosetta spacecraft¹². In that case, a neutral gas cloud was actually discovered and the reason why such outgassing material was staying around the spacecraft is still not clearly understood. The possibility that the low-energy ion observations by BC could actually be determined by ionization and acceleration processes occurring on such a neutral gas cloud needs more investigations, so that several cruise campaigns have been planned to see when and in which conditions such a phenomenon is actually observed. Outbound from Mercury, the about 550 eV slow solar wind is again observed when BC returned to cross the bow shock.

3. Magnetosheath and inner magnetosphere observations.

The inbound bow shock crossing occurred before MIPA and PICAM were turned ON (after the wheel off-loading -WOL- operations). As shown in Fig. 5 (panel b), immediately after switch-on at 22:35 UT MIPA observed a weak signal at 800 eV–1 keV, corresponding to relatively hot magnetosheath population just barely observable within the MIPA FoV perpendicular to the Sun direction. As the spacecraft was moving upstream and closer to the planet, the ion temperature increased and a larger fraction of the distribution function was observed by both PICAM and MIPA (panels a and b). In fact, between about 23:10 UT and about 23:25 UT a signature of ion population was clearly observed by both PICAM and MIPA sensors as a wide distribution centered at about 1 keV. This population can be identified as low latitude boundary layer (LLBL)¹³ similarly of what has been observed in the Earth magnetosphere¹⁴, marking the transition between magnetosheath and magnetosphere. Just after this high density and hot signal at around 23:25 UT, the ion density decreased abruptly, possibly indicating that BC was inside the magnetosphere. At about 23:35 UT, the PICAM and MIPA ion intensity increased again (likely corresponding to the crossing of the plasma sheet), and simultaneously the PICAM background noise decreased significantly. This PICAM background noise decrease was observed also during the second Venus fly-

by and it was interpreted as the shielding of galactic cosmic rays induced by the planet. Approaching the planet, where BC moved northward through the dawn flank plasma sheet, both PICAM and MIPA observed ions at energies between 300 eV and 2000 eV, just before the outbound magnetopause crossing occurred around 23:40 UT. Inside the magnetosphere, the only ion species clearly identified by PICAM is ionized hydrogen: further investigations are needed to identify possible presence of planetary ions in the data. This ion population could be the solar wind entered into the dayside magnetosphere and drifting clockwise around the planet viewed from the north rotational pole, i.e., ion grad B or curvature drift directions as with Earth's ring current (e.g. ref. 15) and seen at higher altitudes by MESSENGER^{18,19}. Approaching the dayside magnetopause at dawn, MIPA observed an increase in plasma ion densities and a decrease in the energy. This clear signature of dayside magnetosheath was registered only by MIPA between 23:40 UT and 23:45 UT (Fig. 5, panel b), while PICAM was switching its operation mode between 23:38 and 23:46 UT. In this observation, the magnetopause and bow shock crossings were registered at distances of 1.5 R_M and 4 R_M , respectively, which is closer to the planet with respect to the average MESSENGER positions for these boundaries (Fig. 2). The predicted crossing times for the bow shock and for the outbound magnetopause are about one to two minutes (note that the MIPA time resolution is 22 s) after the MFB1 observations by SERENA ion sensors.

Discussion

In the present paper we report on the observation of the ion distributions in the environment of planet Mercury, at energies up to 15 keV, as detected by the sensors SERENA-PICAM and -MIPA, during the BC MFB1, on 1st October 2021. The data presented are ion observations in the southern hemisphere of the planet, down to an altitude of about 200 km, the closest approach during MFB1. The solar wind observed by SERENA before and after the magnetospheric crossing reveals the presence of a quite low-energy solar wind of about 500–600 eV. Moreover, we report the observation of intermittent events of high-energy solar wind pulses at about 1500 eV, which were observed during the inbound phase, far outside the bow shock, possibly due to the passage of an interplanetary flux rope. In addition, the outbound observation of the solar wind after the bow shock crossing revealed the presence of two beam-like signals at about 60 eV. This low-energy ion signal (which could be associated with satellite outgassing) is present in PICAM observations only outside the Mercury's Magnetosphere, and well separated from the higher energy solar wind signal. Hence, there is no indication that the observation of planetary plasma by PICAM could be affected by this phenomenon. Both the energetic spikes and the low-energy signals will be investigated in dedicated studies. Inside of Mercury's nightside magnetosphere, protons with energies of one to several keV are observed at low altitudes in the region where a weak ring current composed of drifting ions and electrons has been hypothesized^{15,16}. These initial BC PICAM and MIPA data provide evidence for ring current-like distribution plasma around Mercury, as tentatively reported by MESSENGER data¹⁷, and reviews^{18,19}. Further, the MIPA observations revealed a strong increase in plasma ion densities near the dawn magnetopause, slightly upstream of the terminator plane. Such increases in plasma beta (ratio of plasma thermal energy to magnetic energy) on the dawn side of Mercury's magnetosphere were also observed by MESSENGER during their flybys^{20,21}. These new PICAM and MIPA observations appear to confirm the presence of this unexpected dayside magnetospheric asymmetry, tentatively reported by MESSENGER. Further analysis of the PICAM and MIPA measurements may lead the identification of its formation mechanism that is still eluded in the analyses of magnetosphere observations, e.g. double magnetopause²², sunward transport of plasma sheet plasma²³ or a solar wind-driven low

latitude boundary layer¹³. To summarize, SERENA ion sensors PICAM and MIPA detected various plasma regimes inside Mercury's magnetosphere, possibly allowing the identification of specific ion species and plasma populations, typical of plasma sheet, magnetosheath and magnetopause, up to the bow-shock crossing during the outbound phase. The relevance of these measurements emphasize the importance of the SERENA positive ion sensors. Once their data will be analyzed together with the MAG instrument magnetic field data and other instruments on board Mio and MPO, they will reveal important insight into many unknown aspects of a magnetosphere deep inside the inner heliosphere, like the case of Mercury. The observed plasma regions and features will be investigated in more detail by using new observations from the forthcoming five new Mercury flybys and the nominal phases in Mercury's orbit starting in 2026²⁴.

Data availability

The data referring to BC trajectory in Fig. 1, Fig. 2, and Fig. 3 are provided in the Source Data file. The SERENA raw data shown in Fig. 2, Fig. 4 and Fig. 5 are still in the proprietary period, due to BepiColombo data privacy regulations and cannot be distributed. Presently, these data may be only accessed via authorization in the SERENA team archive upon reasonable request to the SERENA team (PI, Stefano Orsini, stefano.orsini@inaf.it; or PI Deputy, Anna Milillo, anna.milillo@inaf.it). The data are expected to be available in the ESA PSA archive (<https://archives.esac.esa.int/psa/#!Home%20View>) before end of 2024. Source data are provided with this paper.

Code availability

The codes related to the BC trajectory and to the SERENA raw data shown in Fig. 1, Fig. 2, Fig. 3, Fig. 4 and Fig. 5 are still in the proprietary period, due to BepiColombo data privacy regulations and cannot be distributed. Presently, these codes may be only accessed via authorization in the SERENA team archive upon reasonable request to the SERENA team (PI, Stefano Orsini, stefano.orsini@inaf.it; or PI Deputy, Anna Milillo, anna.milillo@inaf.it). The codes are expected to be available in the ESA PSA archive (<https://archives.esac.esa.int/psa/#!Home%20View>) before end of 2024.

References

1. Strom, R. G. & Sprague A. L. *Exploring Mercury: The Iron Planet* (Springer, New York, 2003).
2. Solomon, E. C., McNutt, R. L. Jr, Gold, R. E. & Domingue, D. L. MESSENGER mission overview. *Space Sci. Rev.* **131**, 3–39 (2007).
3. Ness, N. F., Behannon, K. W., Lepping, R. P., and Whang, Y. C. Magnetic field of mercury confirmed. *Nature* **255**, 204 (1975).
4. Anderson, B. J. et al. The global magnetic field of Mercury from messenger orbital observations. *Science* **333**, 1859–1862 (2011).
5. Slavin, J. A., Imber, S. M., Raines, J. M., Dungey, A. in *Space Physics and Aeronomy Collection Volume 2: Magnetospheres in the Solar System* (eds Paxtron, L. J. et al.) Ch. 34 (Wiley, 2021).
6. Benkhoff, J. et al. 'BepiColombo-mission overview and science goals'. *Space Sci. Rev.* **217**, 90 (2021).
7. Mangano et al. 'BepiColombo science investigations during Cruise and Flybys at the Earth, Venus and Mercury'. *Space Sci. Rev.* **217**, 23 (2021).
8. Orsini, S. et al. 'SERENA: Particle instrument suite for determining the sun-mercury interaction from BepiColombo'. *Space Sci. Rev.* **217**, 11 (2021).
9. Jarvinen, R. et al. 'Ultra-low frequency waves in the ion foreshock of Mercury: a global hybrid modeling study'. *Mon. Notices Royal Astron. Soc.* <https://doi.org/10.1093/mnras/stz3257> (2020).
10. Müller, D. et al. The solar orbiter mission. *Sci. Overview* <https://doi.org/10.1051/0004-6361/202038467> (2020).

11. Graf, S. et al. 'Sources for high pressure and contamination at the payload location'. *J. Spacecr. Rockets* **45**, 57 (2008).
12. Schläppi, B. et al. 'Influence of spacecraft outgassing on the exploration of tenuous atmospheres with in situ mass spectrometry'. *J. Geophys. Res.* **115**, A12313 (2010).
13. Anderson, B. J. et al. 'The dayside magnetospheric boundary layer at Mercury. Planet'. *Space Sci. Rev.* **59**, 2037–2050 (2011).
14. Eastman, T. E. et al. The magnetospheric boundary layer: site of plasma momentum and energy transfer from the magnetosheath into the magnetosphere. *Geophys. Res. Lett.* **3**, 685021 (1976).
15. Mura, A. et al. 'Neutral atom imaging at Mercury'. *PSS* **54**, 144–152 (2006).
16. Schriver, D. et al. 'Quasi-trapped ion and electron populations at Mercury'. *Geophys. Res. Lett.* **38**, L23103 (2011).
17. Zhao, J. T. et al. Observational evidence of ring current in the magnetosphere of Mercury. *Nat. Commun.* **13**, 924 (2022).
18. Raines, J. M. et al. 'Plasma sources in planetary magnetospheres: mercury'. *Space Sci. Rev.* **192**, 91–144 (2015).
19. Slavin, J. A. et al.: in 'Mercury's Dynamic Magnetosphere'. *Mercury: The View After MESSENGER* (eds Solomon, S. C., Nittler, L. R. & Anderson, B. J.), Ch. 17 (Cambridge Univ. Press, 2018).
20. Raines, J. M. et al. 'Distribution and compositional variations of plasma ions in Mercury's space environment: the first three Mercury years of MESSENGER observations'. *J. Geophys. Res.* **118**, 1604–1619 (2013).
21. Slavin, J. A. et al. 'Mercury's magnetosphere after MESSENGER's first Flyby'. *Science* **321**, 85–89 (2008).
22. Muller, J. et al. 'Origin of Mercury's double magnetopause: 3D hybrid simulation with A.I.K.E.F.'. *Icarus* **218**, 666–687 (2012).
23. Shi, Z. et al. An eastward current encircling Mercury. *Geophys. Res. Lett.* **49**, e2022GL098415 (2022).
24. Milillo, A. et al. 'Investigating Mercury's environment with the two-spacecraft BepiColombo mission'. *Space Sci. Rev.* <https://doi.org/10.1007/s11214-020-00712-8> (2020).
25. Winslow, R. et al. 'Mercury's magnetopause and bow shock from MESSENGER Magnetometer observations'. *J. Geophys. Res.* **118**, 2213–2227 (2013).
26. Slavin, J. A. et al. 'MESSENGER observations of magnetic reconnection in mercury's magnetosphere'. *Science* **324**, 606 (2009).
- (G.L.), H. Nilsson (H.N.), M. Phillips (M.P.), A. Aronica (A.A.), E. Kallio (E.K.), P. Wurz (P.W.), T. Alberti (T.A.), A. Olivieri (A.O.), C. Plainaki (C.P.), J. A. Slavin (J.A.S.), I. Dandouras (I.D.), J. M. Raines (J.M.R.), J. Benkhoff (J.Be.), J. Zender (J.Z.), J.-J. Berthelier (J.-J.B.), M. Dosa (M.Do.), G. C. Ho (G.C.H.), R. M. Killen (R.M.K.), S. McKenna-Lawlor (S.M.-L.), K. Torkar (K.T.), O. Vaisberg (O.V.), F. Allegrini (F.A.), I. A. Daglis (I.A.D.), C. Dong (C.D.), C. P. Escoubet (C.P.E.), S. Fatemi (S.F.), M. Fränz (M.F.), S. Ivanovski (S.I.), H. Lammer (H.La.), François Leblanc (Fra.L.), V. Mangano (V.M.), A. Mura (A.Mu.), R. Rispoli (R.R.), M. Sarantos (M.S.), H. T. Smith (H.T.S.), M. Wieser (M.W.), F. Camozzi (F.C.), A. M. Di Lellis (A.M.D.L.), G. Fremuth (G.F.), F. Giner (F.G.), R. Gurnee (R.G.), J. Hayes (J.H.), H. Jeszenszky (H.J.), B. Trantham (B.T.), J. Balaz (J.Ba.), W. Baumjohann (W.B.), M. Cantatore (M.C.), D. Delcourt (D.D.), M. Delva (M.Del.), M. Desai (M.Des.), H. Fischer (H.F.), A. Galli (A.G.), M. Grande (M.G.), M. Holmström (M.H.), I. Horvath (I.H.), K.C. Hsieh (K.C.H.), R. Jarvinen (R.J.), R. E. Johnson (R.E.J.), A. Kazakov (A.K.), K. Kecskemeti (K.K.), H. Krüger (H.K.), C. Kürbisch (C.K.), Frederic Leblanc (Fre.L.), M. Leichtfried (M.L.), E. Mangraviti (E.M.), S. Massetti (S.M.), D. Moissenko (D.M.), M. Moroni (M.M.), R. Noschese (R.N.), F. Nuccilli (F.N.), N. Paschalidis (N.P.), J. Ryno (J.R.), K. Seki (K.Se.), A. Shestakov (A.S.), S. Shuvalov (S.Sh.), R. Sordini (R.S.), F. Stenbeck (F.S.), J. Svensson (J.S.), S. Szalai (S.Sz.), K. Szego (K.Sz.), D. Toubanc (D.T.), N. Vertolli (N.V.), R. Wallner (R.W.), A. Vorburger (A.Vo.). Conceptualization: S.O., A.Mi., H.Li., A.Va., S.B., S.L.; methodology: S.O., A.Mi., H.Li., A.Va., S.B., S.L., A.A.; investigation: S.O., A.Mi., A.Vo., S.B., E.D.A., G.L., H.N., E.K., P.W., T.A., J.A.S., J.M.R., I.D.; visualization: S.O., A.Mi., A.Va., S.B., E.D.A., E.K., J.A.S., A.A.; funding acquisition: A.O., S.O., A.Mi., H.Li., A.Va., S.B., S.L.; project administration: A.O., S.O., A.Mi., H.Li., A.Va., S.B., S.L.; supervision: S.O.; writing original draft: S.O., A.Mi., H.Li., A.Va., S.B., S.L., E.D.A., G.L., H.N., M.P., A.A., E.K., P.W., T.A., A.O., C.P., J.A.S., I.D., J.M.R.; writing review and editing: S.O., A.Mi., H.Li., A.Va., S.B., S.L., E.D.A., G.L., H.N., M.P., A.A., E.K., P.W., T.A., A.O., C.P., J.A.S., I.D., J.M.R., J.Be., J.Z., J.-J.B., M.Do., J.H., R.M.K., S.M.-L., K.T., O.V., F.A., I.A.D., C.D., C.P.E., S.F., M.F., S.I., H.La., Fra.L., V.M., A.Mu., R.R., M.S., H.T.S., M.W., F.C., A.M.D.L., G.F., F.G., R.G., J.H., H.J., B.T., J.Ba., W.B., M.C., D.D., M.Del., M.Des., H.F., A.G., M.G., M.H., I.H., K.C.H., R.J., R.E.J., A.K., K.K., H.K., C.K., Fre.L., M.L., E.M., S.M., D.M., M.M., R.N., F.N., N.P., J.R., K.Se., A.S., S.Sh., R.S., F.S., J.S., S.Sz., K.Sz., D.T., N.V., R.W., A.Vo.

Acknowledgements

SERENA general management, System Control Unit (SCU) and Emitted Low Energy Neutral Atoms (ELENA) unit are funded by the Italian Space Agency (ASI) and by the Italian National Institute of Astrophysics (INAF), agreement n. 2018-8-HH.O. SERENA ground-based activity is also funded by the Expert support to SERENA Science Operations (EXPRO), ESA Contract Nr. C4000119196/16/ES/JD. Strofio unit is funded by NASA, through Marshall Space Flight Center under the Discovery Program Office. PICAM is funded mostly by the Austrian Space Applications Programme (ASAP) of the Austrian Research Promotion Agency (FFG), and partially by the Programme de Développement d'Expériences (PRODEX), and by the French Space Agency (CNES). MIPA is funded by the Swedish National Space Agency. Strofio and MIPA, as well as the general SERENA suite ground testing activities, have been also supported by the University of Bern, Switzerland.

Author contributions

S. Orsini (S.O.), A. Milillo (A.Mi.), H. Lichtenegger (H.Li.), A. Varsani (A.Va.), S. Barabash (S.B.), S. Livi (S.L.), E. De Angelis (E.D.A.), G. Laky

Competing interests

The authors declare no competing interests.

Additional information

Supplementary information The online version contains supplementary material available at <https://doi.org/10.1038/s41467-022-34988-x>.

Correspondence and requests for materials should be addressed to S. Orsini.


















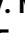

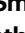









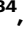


Peer review information *Nature Communications* thanks David Schriver, and the other, anonymous, reviewers for their contribution to the peer review of this work.

Reprints and permissions information is available at <http://www.nature.com/reprints>

Publisher's note Springer Nature remains neutral with regard to jurisdictional claims in published maps and institutional affiliations.

Open Access This article is licensed under a Creative Commons Attribution 4.0 International License, which permits use, sharing, adaptation, distribution and reproduction in any medium or format, as long as you give appropriate credit to the original author(s) and the source, provide a link to the Creative Commons license, and indicate if changes were made. The images or other third party material in this article are included in the article's Creative Commons license, unless indicated otherwise in a credit line to the material. If material is not included in the article's Creative Commons license and your intended use is not permitted by statutory regulation or exceeds the permitted use, you will need to obtain permission directly from the copyright holder. To view a copy of this license, visit <http://creativecommons.org/licenses/by/4.0/>.

© The Author(s) 2022

S. Orsini ¹✉, **A. Milillo** ¹, **H. Lichtenegger**², **A. Varsani** ², **S. Barabash**³, **S. Livi**^{4,5}, **E. De Angelis**¹, **T. Alberti**¹, **G. Laky**², **H. Nilsson**³, **M. Phillips** ⁴, **A. Aronica** ¹, **E. Kallio** ⁶, **P. Wurz** ⁷, **A. Olivieri** ⁸, **C. Plainaki**⁸, **J. A. Slavin** ⁵, **I. Dandouras** ⁹, **J. M. Raines**⁵, **J. Benkhoff** ¹⁰, **J. Zender**¹⁰, **J.-J. Berthelier**¹¹, **M. Dosa**¹², **G. C. Ho** ¹³, **R. M. Killen** ¹⁴, **S. McKenna-Lawlor**¹⁵, **K. Torkar**², **O. Vaisberg**¹⁶, **F. Allegrini**^{4,17}, **I. A. Daglis** ^{18,19}, **C. Dong** ²⁰, **C. P. Escoubet**¹⁰, **S. Fatemi** ²¹, **M. Fränz** ²², **S. Ivanovski**²³, **N. Krupp**²², **H. Lammer**², **François Leblanc**¹¹, **V. Mangano** ¹, **A. Mura**¹, **R. Rispoli** ¹, **M. Sarantos**¹⁴, **H. T. Smith**¹³, **M. Wieser** ³, **F. Camozzi**²⁴, **A. M. Di Lellis**²⁵, **G. Fremuth**², **F. Giner**², **R. Gurnee**²⁶, **J. Hayes**¹³, **H. Jeszenszky**², **B. Trantham**², **J. Balaz** ²⁷, **W. Baumjohann**², **M. Cantatore** ²⁴, **D. Delcourt**²⁸, **M. Delva**², **M. Desai**⁴, **H. Fischer**²², **A. Galli** ⁷, **M. Grande** ²⁹, **M. Holmström**³, **I. Horvath**¹², **K. C. Hsieh**³⁰, **R. Jarvinen** ^{6,31}, **R. E. Johnson**³², **A. Kazakov** ¹, **K. Kecskemeti**¹², **H. Krüger**²², **C. Kürbis**², **Frederic Leblanc**³³, **M. Leichtfried**², **E. Mangraviti**²³, **S. Massetti** ¹, **D. Moissenko** ¹⁶, **M. Moroni**¹, **R. Noschese**¹, **F. Nuccilli**¹, **N. Paschalidis**¹⁴, **J. Ryno** ³¹, **K. Seki** ³⁴, **A. Shestakov**¹⁶, **S. Shuvalov** ¹⁶, **R. Sordini** ¹, **F. Stenbeck**³, **J. Svensson**³, **S. Szalai**¹², **K. Szego**^{12,35}, **D. Toubanc**⁹, **N. Vertolli**¹, **R. Wallner**² & **A. Vorburger**⁷

¹Institute of Space Astrophysics and Planetology, INAF, Roma, Italy. ²Space Research Institute, Austrian Academy of Sciences, Graz, Austria. ³Swedish Institute of Space Physics, Kiruna, Sweden. ⁴Southwest Research Institute, San Antonio, TX, USA. ⁵University of Michigan, Department of Climate and Space Sciences and Engineering, Ann Arbor, MI, USA. ⁶Aalto University, Department of Electronics and Nanoengineering, School of Electrical Engineering, Helsinki, Finland. ⁷University of Bern, Institute of Physics, Bern, Switzerland. ⁸Italian Space Agency, ASI, Roma, Italy. ⁹Institut de Recherche en Astrophysique et Planétologie, CNRS, CNES, Université de Toulouse, Toulouse, France. ¹⁰ESA-ESTEC, Noordwijk, The Netherlands. ¹¹LATMOS/IPSL, CNRS, Sorbonne Université, Paris, France. ¹²Wigner Research Centre for Physics, Budapest, Hungary. ¹³The Johns Hopkins University Applied Physics Laboratory, Laurel, MD 20723, USA. ¹⁴NASA/Goddard Space Flight Center, Greenbelt, MD 20771, USA. ¹⁵Space Technology Ireland, Ltd., Maynooth, Co., Kildare, Ireland. ¹⁶IKI Space Research Institute, Moscow, Russia. ¹⁷University of Texas at San Antonio, Department of Physics and Astronomy, San Antonio, TX, USA. ¹⁸National and Kapodistrian University of Athens, Department of Physics, Athens, Greece. ¹⁹Hellenic Space Center, Athens, Greece. ²⁰Princeton Plasma Physics Laboratory and Department of Astrophysical Sciences, Princeton University, Princeton, NJ, USA. ²¹Department of Physics, Umeå University, Umeå, Sweden. ²²Max-Planck-Institut für Sonnensystemforschung, MPS, 37077 Göttingen, Germany. ²³Astronomical Observatory, INAF, Trieste, Italy. ²⁴OHB-Italia SpA, Milano, Italy. ²⁵AMDL srl, Roma, Italy. ²⁶Laboratory for Atmospheric and Space Physics, Boulder, CO, USA. ²⁷Institute of Experimental Physics SAS, Slovak Academy of Sciences, 040 01 Košice, Slovakia. ²⁸Université d'Orléans, Orléans, France. ²⁹Aberystwyth University, Aberystwyth, Ceredigion, UK. ³⁰University of Arizona, Tucson, AZ, USA. ³¹Finnish Meteorological Institute FMI, Helsinki, Finland. ³²University of Virginia, Charlottesville, VA 22904, USA. ³³LPP, École polytechnique, 91128 Palaiseau Cedex, Paris, France. ³⁴University of Tokyo, Department of Earth and Planetary Science, Graduate School of Science, Tokyo, Japan.

³⁵Deceased: Karoly Szego ✉ e-mail: stefano.orsini@inaf.it

Inner southern magnetosphere observation of Mercury via SERENA ion sensors in BepiColombo mission

S. Orsini^{1*}, et al.

1. Institute of Space Astrophysics and Planetology, INAF, Rome, Italy.

*Corresponding author: stefano.orsini@inaf.it

Supplementary Information

Methods

- Data Downlink and processing data pipeline

Payload telemetry (P/L TM) data collected by BC is downlinked to Earth through the Estrack ground stations antennas of ESA

(https://www.esa.int/Enabling_Support/Operations/ESA_Ground_Stations/Estrack_ground_stations)

and the Deep Space Network (DSN) antennas of NASA Ground Segment

(https://www.nasa.gov/directorates/heo/scan/services/networks/deep_space_network/about).

From there, data are transferred and stored at the Ground Operation System's Data Dissemination System (EDDS) server located at ESA-ESOC (Germany) where they are ready to be retrieved directly by the instrument teams or by the ESA Science Ground Segment (SGS) servers located at ESA-ESAC (Spain). P/L TM is binary data produced according to the SCOS-2000 standard

(https://www.esa.int/Enabling_Support/Operations/Ground_Systems_Engineering/SCOS-2000).

They basically consist of science (SC) measurements and instrument housekeeping (HK) data. Once received on-ground, TM data are sorted by generation time (Spacecraft (S/C) Elapsed Time - SCET-), packed and stored into the EDDS server, and finally provided to the instrument teams and SGS team as DDS binary data. SERENA team has developed a scientific data processing and archiving architecture in cooperation with BC SGS team. The SERENA instrument pipeline is developed by the SERENA team. As for any other BepiColombo Instrument (e.g. 1), it basically consists of two main routines: telemetry-to-raw (TM2RAW) and raw-to-calibrated (RAW2CAL), generating all HK and SC instrument data, and in some additional sub-routines generating ancillary data (e.g. documentation, geometry files, ...). Only the TM2RAW routine has been implemented into the pipeline so far, while RAW2CAL routine is under development and will be implemented soon. For this reason, a reference to this work is still not available, but an article will be issued as soon as the pipeline is completed. The pipeline is designed to run at both INAF-IAPS and SGS, and provides validated data sets and a quick-look analysis tool. Data processed by the pipeline are formatted according to the Planetary Data System, Version 4 standards (PDS4,

<https://pds.nasa.gov/datastandards/about/> and [https://www.cosmos.esa.int/web/psa/pds4-](https://www.cosmos.esa.int/web/psa/pds4-standards)

[standards](https://www.cosmos.esa.int/web/psa/pds4-standards)), maintained by NASA, and archived into the public Planetary Science Archive (PSA,

<https://www.cosmos.esa.int/web/psa/psa-introduction>), maintained by ESA. The pipeline has two different processing branches: telemetry-to-raw (TM2RAW) data and raw-to-calibrated (RAW2CAL) data. The former generates RAW data from the TM files, the latter uses RAW data to produce CALibrated data. Usually, the two modules work in sequence, but they can also work separately, e.g. for instrument health checks (TM2RAW) or re-calibration purposes (RAW2CAL). The inputs of TM2RAW are the DDS files retrieved by the S/C and the SPICE kernels provided by the NASA's Navigation and Ancillary Information Facility (NAIF) team

(<https://naif.jpl.nasa.gov/naif/spiceconcept.html>). The TM2RAW routine extracts all relevant binary data packets (SC and HK) from DDS files, generates proper UTC time stamps, and converts the data into ASCII RAW data files. The SPICE kernels contain the information to calculate the spacecraft position, the FoV of the sensors and the parameters for the time conversions for each SC and HK packet. Additionally, PDS4 label files in XML format are generated to provide ancillary information. The RAW data includes unprocessed (ADC counts) original SC and HK data from the instrument which is mainly used for diagnostic purposes. If compression, reformatting, packetization, or other translation has been applied to facilitate data transmission or storage, all data generated by the pipeline are available as ASCII files and grouped in RAW, CALIBRATED & DERIVED data. Below this level, data are grouped by mission phases, e.g.: Near Earth Commissioning or Cruise. The next logical level distinguishes data sensor by sensor, and then separates the housekeeping HK from science SC data. Additionally, browse plots for a quick data

overview and useful information for the data end-user can be found in the archived datasets. In the present paper only RAW data are shown.

- PICAM (Planetary Ion CAMera) ion mass spectrometer)

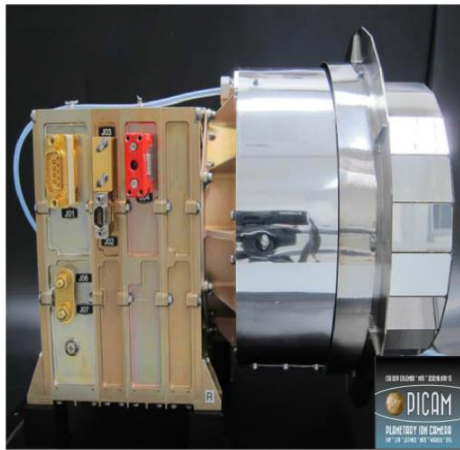
PICAM is an all-sky camera (1, 3) capable of measuring the 3D velocity distribution of ions up to ~3 keV energies, and their mass spectrum extending up to ~132 amu (Xenon). SERENA-PICAM is an omnidirectional sensor with no angular scanning, hence having a very efficient duty cycle. A photo of the flight hardware is illustrated in Supplementary Figure 1, and its specification, such as field of view (FoV), energy range, geometrical factor and mass resolution are represented in Supplementary Table 1. More details regarding the instrument design, operational modes, calibration tests and science objectives are explained in (3). During BepiColombo first flyby at Mercury, SERENA-PICAM was chosen to operate in two major modes, Image (IMG) and Time of Flight (ToF). The IMG mode provided ion counts for 32 energy channels, and 31 anodes. The IMG mode was operated in Solar Wind covering 460 to 2100 eV, and at Bowshock from 11 to 2735 eV. Near the planet, SERENA-PICAM switched to ToF mode with the latter energy range, but a high mass resolution to look at the planetary ion species. The boresight vector of PICAM was perpendicular to the Sun-MPO line throughout the flyby. The details of each mode are also shown in Supplementary Table 1.

- MIPA (Miniature Ion Precipitation Analyzer)

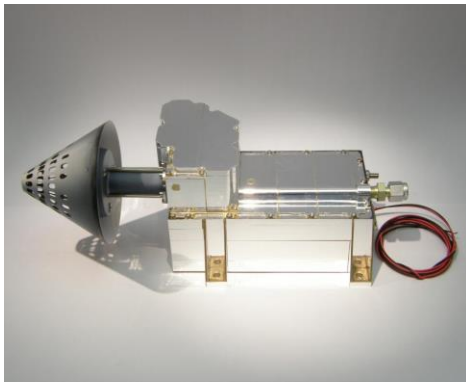
MIPA (Supplementary Figure 2) is a highly optimized compact (~600 g) ion mass analyzer of the SWIP-family (4, 3) capable of measuring the 3D velocity distribution of ions in the energy range 10 eV – 15 keV with mass resolution to resolve the main plasma species (1,2,4,8,> 16 amu). MIPA is a single pixel fast sweeping sensor (8 ms sampling time per energy level) capable of covering 96 energies x 24 directions for just 18 sec (full mode). MIPA uses ion – surface interaction combined with the time-of-flight (TOF) analysis of the secondary electrons for the ion mass determination. MIPA does not have its own data processing and is controlled by the SERENA processing unit. Supplementary Table 2 sums up the basic performances. During the time interval used in this analysis MIPA operated in the full angular coverage mode (24 viewing pixels) for 32 energy steps (3 steps integrated) with fastest time resolution (20 sec /3d, 18 sec + 2 sec idle, no time integration). 8 TOF bins were used which is sufficient to resolve hydrogen and heavy ions (≥ 2 amu)

References

1. Heyner, D., et al.: The BepiColombo Planetary Magnetometer MPO-MAG: what can we learn from the Hermean Magnetic Field?. *Space Science Reviews* (2021) 217:52, <https://doi.org/10.1007/s11214-021-00822-x>
2. Vaisberg, O., et al.: 'The 2π charged particles analyzer: all-sky camera concept and development for space missions'. *J Geophys Res*, 121(12), 11750–11765 (2001). <https://doi.org/10.1002/2016JA022568>.
3. Orsini, S., et al.: 'SERENA: Particle Instrument Suite for Determining the Sun-Mercury Interaction from BepiColombo'. *Space Sci Rev*, 217, 11 (2021). <https://doi.org/10.1007/s11214-020-00787-3>.
4. Wieser, M., S. Barabash: 'A family for miniature, easily reconfigurable particle sensors for space plasma measurements', *J Geophys Res* (2016). <https://doi.org/10.1002/2016JA022799>.



Supplementary Figure 1. **Side view of the PICAM flight model**



Supplementary Figure 2. **MIPA flight model.** The aperture is protected by the conic radiator with entrance holes. The hot section (radiator and angular sweeping electrodes inside) operates at 400°C and is decoupled from the rest of the instrument by a titanium decoupling tube.

Energy range	~10 - 3000 eV	Run time [minute]	995	80	90
Energy resolution ($\Delta E/E$)	<15%	Science region	Solar Wind	Magnetosphere	Bowshock , Solar Wind
Viewing angle	3D, 1.5π				
Angular resolution	~20° x 60°	PICAM mode	IMG 4	ToF 11 (S)	IMG 4
Mass range	1-132 AMU	No. of anodes	31	4	31
Mass resolution ($M/\Delta M$)	> 50	ToF bins	NA	512 bins	NA
Time resolution	<1 m	Energies measured	460-2100 eV (32 ch.)	11-2735 eV (32 ch.)	11-2735 eV (32 ch.)
Sampling time	1-320 s				
Effective Geo. factor ($S \Omega \Delta E/E$)	$10^{-4} - 10^{-6}$ (cm ² sr eV)/eV	Temporal resolution [s]	64	128	64

Supplementary Table 1. **PICAM specifications.** The left half represents the general specifications for SERENA-PICAM, and the right half the operational details of SERENA-PICAM during the first Mercury Flyby.

Parameter	Value
Energy range	10 eV – 15 keV
Energy resolution $\Delta E/E$	7.3%
Viewing angle	90° x 180°
Angular resolution (variable)	40°x20° (max pixel) 5° x 15 (min pixel)
Mass range, amu	1 - 50
Mass resolution, $M/\Delta M$	2-5
Time resolution, sec	18, Full Angular– Energy cycle (24A x 96E)
Efficiency, ϵ	12%
Geometrical factor, w/o ϵ , maximum possible base line	$24 \times 2 \cdot 10^6 \text{ cm}^2 \text{ sr eV/eV}$
Dynamical range	$2 \cdot 10^7$

Supplementary Table 2. **MIPA basic performances**